Rheol Acta (2015) 54:601–618
DOI 10.1007/s00397-015-0855-x

ORIGINAL CONTRIBUTION

Large amplitude oscillatory shear rheology of three different shear-thickening particle dispersions

Sunilkumar Khandavalli[1] · Jonathan P. Rothstein[1]

Received: 21 August 2014 / Revised: 30 March 2015 / Accepted: 2 April 2015 / Published online: 10 May 2015

Abstract We present a large amplitude oscillatory shear rheology (LAOS) investigation of three different shear-thickening particle dispersions - fumed silica in polyethylene oxide (*FLOC*), fumed silica in polypropylene glycol (*HydroC*), and cornstarch in water (*JAM*). These systems shear-thicken by three different mechanisms - shear-induced formation of particle clusters flocculated by polymer bridging, hydrocluster formation, and jamming. The viscoelastic non-linearities of the three fluids were studied as a function of strain and strain-rate space through the use of Lissajous-Bowditch curves and local nonlinear viscoelastic moduli of an oscillatory shear cycle. The nonlinear behaviors of the three fluids were compared and contrasted to understand the nonlinear shear-thickening mechanism of each. Both *HydroC* and *JAM* dispersions were found to exhibit strong strain stiffening of the elastic moduli and strain thickening of the loss moduli behavior associated with possible hydrocluster formation and particle jamming. However, the *FLOC* dispersion, in contrast, showed strong strain softening and strain thinning behavior at large strain amplitudes associated with yielding of the microstructure. The expected thickening of the loss modulus of *FLOC* in LAOS with increasing strain was not observed even though viscosity of *FLOC* was found to shear-thicken in steady-shear measurements. This disagreement is likely due to very large strain amplitudes required for shear-thickening to occur by shear-induced polymer bridging mechanism. The hypothesis was confirmed through stress growth experiments. Conversely, the *HydroC* and *JAM* dispersions required relatively small applied strains for shear-thickening to occur by hydrocluster and jamming mechanism. The comparison of local intra-cycle nonlinearity through Lissajous-Bowditch plots and nonlinear viscoelastic parameters indicated that the elastic nonlinearities of all three systems are primarily driven by a strong dependence on the magnitude of the applied strain-rates within an oscillatory cycle rather than the amplitude of the applied strain. A close inspection of the LAOS data reveals strong differences in the viscoelastic nonlinearities of these three different shear-thickening dispersions which can be used to create a nonlinear rheological fingerprint for each and offers valuable new insights into the nonlinear dynamics associated with each of the shear-thickening mechanisms.

Keywords Colloids · Suspension · Shear-thickening · Non-linear rheology · Large amplitude oscillatory shear (LAOS)

✉ Jonathan P. Rothstein
rothstein@ecs.umass.edu

Sunilkumar Khandavalli
skhandav@umass.edu

[1] Department of Mechanical and Industrial Engineering, University of Massachusetts Amherst, Amherst, MA 01003, USA

Introduction

Particle dispersions are ubiquitous in every day life. These rheologically complex fluids are found in a host of materials ranging from detergents, paints, food, cements, and pharmaceuticals. Shear-thickening dispersions are one interesting class of fluids, which are of enormous amount

of interest in both academia (Barnes 1989) and industry (Wagner and Brady 2009). In a shear-thickening fluid, the viscosity abruptly increases with increasing shear rate. A classic example is the cornstarch and water mixture known as "oobleck". Shear thickening can often have consequences in fluid handling causing damage in industrial processes by breaking equipment or fouling spraying equipment and pumps. Still when properly designed and handled, shear-thickening fluids have been exploited for a wide range of innovative applications. Examples of these applications include developing bullet proof soft body armor (Lee and Wagner 2003), machine mounts and damping devices (Helber et al. 1990; Laun et al. 1991), and driving fluids for enhanced oil recovery (Nilsson et al. 2013).

Shear-thickening in particle dispersions can occur by various mechanisms depending on the range of particle volume fraction (Fall et al. 2008) and the nature of solvent phase (Raghavan and Khan 1997; Kamibayashi et al. 2008). In Brownian dispersions stabilized by electrostatic or steric forces, for particle concentrations ranging from small to medium particle volume fractions, shear-thickening occurs due to the formation of hydroclusters (Wagner and Brady 2009). These dense particle clusters of tightly packed particles are held together by hydrodynamic interactions (Bossis and Brady 1984, 1989). Beyond certain shear-rate, the hydrodynamic lubrication forces dominate all the other colloidal forces resulting in the formation of hydroclusters. The resulting anisotropy in the colloidal dispersions gives rise to large stress fluctuations and as a result large shear viscosities (Melrose and Ball 2004). The magnitude and the critical shear-rate for the onset of the shear-thickening are influenced by several factors such as the thickness of polymer grafted layer, polymer molecular weight, particle size, particle surface chemistry, and the viscosity of solvent medium (Shenoy and Wagner 2005; Frith et al. 1996; Mewis and Biebaut 2001; Mewis and Vermant 2000; Galindo-Rosales and Rubio-Hernàndez 2010).

Partial stabilization of dispersion by the adsorption of large molecular weight polymer can also cause shear-thickening. The free ends of the adsorbed polymer chains can interact with the neighboring particles by bridging to one or more particles. During flow, the shear fields facilitate interaction between polymer chains and particles causing flocculation of the particles by bridging with polymer chains. The formation of such flocculated particle clusters causes shear-thickening (Kamibayashi et al. 2008). The shear-thickening behavior depends on a number of factors including, the particle concentration, size, polymer concentration, and molecular weight (Kamibayashi et al. 2008; Khandavalli and Rothstein 2014; Otsubo 2001).

In dense non-Brownian suspensions, close to random packing fraction, shear-thickening is due to dilatancy and eventual jamming that can result in a solid-like material (Fall et al. 2008, 2010; Brown and Jaeger 2009; Bertrand et al. 2002). To accommodate flow, the particles dilate due to crowding/confinement via the formation a dense jammed network of particle clusters. The dilatancy in hard-sphere dense suspensions is accompanied by a positive normal stress difference (N_1) (Lootens et al. 2005; Cates et al. 2005), distinct from continuous shear-thickening due to pure hydrodynamic forces which exhibit negative normal stress difference (Foss and Brady 2000; Lee et al. 2006). Large stresses due to particle contact/frictional forces associated with the jammed structure are the cause for shear-thickening (Fall et al. 2008, 2010). These jammed structures are dynamic, continuously reforming and breaking up, and are manifested by large stress fluctuations (Larsen et al. 2014) and the discontinuous behavior in shear-thickening (Seto et al. 2013).

The shear-thickening mechanism in Brownian and non-Brownian dense dispersions has been investigated extensively through various techniques including experiments, simulations, and light scattering (Fall et al. 2008; Kamibayashi et al. 2008; Laun et al. 1992; Hoffman 1972; Bossis and Brady 1984). However, studies on viscoelasticity of shear-thickening dispersions, especially the nonlinear shear behavior at large deformations, are limited to steady-shear measurements and the measurements of the fundamental frequency moduli in oscillatory shear. Dynamic oscillatory shear rheology studies on Brownian steric or electrostatically stabilized systems showed strong strain-stiffening behavior in the elastic moduli, G_1', in addition to strain-thickening in the loss moduli, G_1''. The critical strain, in addition to frequency/strain-rate, was found to affect the onset and magnitude of strain-stiffening/thickening (Raghavan and Khan 1997; Fischer et al. 2007; Jiang et al. 2010; Chang et al. 2011) with the data following the Delaware-Rutgers rule. For the case of particle dispersions partially flocculated by polymer bridging, viscoelastic studies both linear (Otsubo and Umeya 1984; Khandavalli and Rothstein 2014) and nonlinear (Otsubo 2001, 1999) indicated that for these systems elasticity have an important role in the shear-thickening mechanism.

There have been several studies examining the nonlinear viscoelasticity of dense suspensions, although none that have been shown to shear-thicken through steady shear rheology measurements (Lin et al. 2013; Nam et al. 2011; Bricker and Butler 2007; Narumi et al. 2005; GadalaMaria and Acrivos 1980). In transient shear and oscillatory shear measurements on dense suspensions, a strong nonlinear response involving a stress undershoot, associated with microstructural rearrangements upon shear reversal has been observed (Narumi et al. 2005; GadalaMaria and Acrivos 1980). Nam et al. (2011) have conducted LAOS experiments on concentrated suspensions of polymethylmethacrylate (PMMA) particles dispersed in

Newtonian fluids and have examined the effect of various factors such as particle volume fractions, medium viscosity, and particle size on the nonlinear behavior. The suspensions were found to show strong strain-stiffening behavior, and the behavior has been attributed to shear-induced collision of particles (Nam et al. 2011). The critical strain amplitude for the onset of strain stiffening was found to decrease with increasing particle volume fraction, but was found to be independent of other factors such as the medium viscosity, imposed angular frequency, and particle size (Nam et al. 2011). There have also been studies on shear-thickening suspensions through shear-cessation and normal stress difference measurements examining the role of elasticity associated with the shear-induced jammed structures and liquid to solid-like transition (Larsen et al. 2014; 2010; O'Brien and Mackay 2000).

The nonlinear viscoelasticity studies of shear-thickening dispersions discussed to this point have been limited only to variations of the moduli associated with the fundamental harmonics of the imposed oscillation frequency. The higher harmonic contributions are often ignored due to their relatively low magnitudes (Otsubo 1999; Raghavan and Khan 1997). However, the viscoelastic nonlinearities due to the higher harmonics can offer important insights into the microstructural and physical mechanisms responsible for the nonlinear rheological response. Additionally, even in the absence of a clear understanding of the physics, often a rheology fingerprint behavior can be ascribed/identified to specific material system through LAOS measurements (Ewoldt et al. 2008; Hyun et al. 2011). Recent developments in nonlinear rheology enabled tools to characterize the large amplitude oscillatory shear behavior through meaningful material parameters and presentation methods (Ewoldt et al. 2008; Hyun et al. 2011; Ewoldt and Bharadwaj 2013). In this study, we present a comparative study of the nonlinear viscoelasticity through large amplitude oscillatory shear (LAOS) measurements of three shear-thickening particle dispersions which thicken by different commonly known mechanisms. These dispersions are sterically stabilized Brownian dispersions, fumed silica in polypropylene glycol; partially stabilized nanoparticle dispersions flocculated by polymer bridging, fumed silica in polyethylene oxide; and dense non-Brownian suspensions, cornstarch in water. The associated shear-thickening mechanisms of the dispersions will be discussed in steady-shear rheology characterization. The small amplitude oscillatory shear behavior was also characterized prior to investigating the large amplitude oscillatory shear behavior. The large amplitude oscillatory shear rheology was characterized for various frequencies and the viscoelastic nonlinearities were studied. The viscoelastic nonlinearities associated with each shear-thickening mechanism were examined while comparing and contrasting between the systems.

Theoretical background

Large amplitude oscillatory shear (LAOS)

In dynamic oscillatory shear rheology, a sinusoidal strain (or stress) signal is imposed on a material given as,

$$\gamma(t) = \gamma_o sin(\omega_1 t), \tag{1}$$

where γ_0 and ω_1 are input strain amplitude and frequency, respectively. For small strain amplitudes, the resulting stress response is also sinusoidal. The linear viscoelastic (LVE) response is represented as

$$\sigma(t) = \sigma_o \sin(\omega_1 t + \delta_1). \tag{2}$$

The above equation can be rewritten as

$$\sigma(t) = \gamma_o \left[G_1'(\omega_1) sin(\omega_1 t) + G_1''(\omega_1) cos(\omega_1 t)\right], \tag{3}$$

where the in-phase and out-of-phase components of the stress response are termed as storage modulus, G_1' and loss modulus, G_1''. When the input strain amplitude is increased beyond a critical value, the stress response becomes nonlinear and can be represented as

$$\sigma(t, \gamma, \omega) = \Sigma \sigma_n sin(n\omega_1 t + \delta_n), \tag{4}$$

where additional higher harmonic stress components ($n > 1$) are present in the stress response. Therefore, the G_1' and G_1'' based on fundamental harmonic do not fully describe the mechanical behavior beyond the LVE limit and the higher harmonics cannot be ignored. One common method to examine a nonlinear response is by performing Fourier transform and examining the frequency spectrum (Wilhelm 1999, 1998). The intensity of higher stress harmonics is an indication of degree of nonlinearity. This method has been a valuable tool for characterizing nonlinear behavior for several materials such as polymer melts, filled rubbers (Leblanc 2008; Leblanc et al. 2011), suspensions, and emulsions (Hyun et al. 2006; Neidhfer et al. 2004; Klein et al. 2008; Hyun et al. 2003). Only odd harmonics appear in the nonlinear region, and the appearance is assumed due to odd symmetry with respect to the directionality of shear strain (Bird et al. 1987). The appearance of even harmonics in Fourier spectrum can be attributed to the presence of secondary flows (Atalik and Keunings 2004), asymmetric wall slip or edge effects (Graham 1995). However, Fourier transform rheology lacks a direct physical interpretation of the material response. Another common method for investigating nonlinear response is graphical approach, where stress versus strain curves known as Lissajous-Bowditch curves are studied. The nonlinear behavior of material can be identified from the shape of Lissajous-Bowditch or stress

versus strain curve, as follows: linear, purely elastic; circle, purely viscous; ellipse, LVE; and distorted ellipse, nonlinear viscoelastic. Thus, the progressive transition from linear to nonlinear viscoelastic nature of the material with strain amplitude can be studied from the graphical representation. The total stress can be further be decomposed into elastic and viscous components through simple algebraic manipulations using even and odd nature of the trignometric functions (Cho et al. 2005). Extending Cho's stress decomposition (Cho et al. 2005) method, Ewoldt et al. (2008) proposed more physically meaningful nonlinear viscoelastic measures through representation of elastic and viscous stresses through orthogonal Chebyshev polynomials of the first kind. Ewoldt et al. (2008) have also defined nonlinear viscoelastic moduli based on local material response at small and large instantaneous strains/strain rates in an oscillatory cycle (Ewoldt et al. 2008). The nonlinear elastic material parameters are given in terms of Fourier coefficients as,

$$G'_M = \left.\frac{d\sigma}{d\gamma}\right|_{\gamma=0} = \sum_{n=odd} nG'_n, \tag{5}$$

$$G'_L = \left.\frac{\sigma}{\gamma}\right|_{\gamma=\pm\gamma_0} = \sum_{n=odd} G'_n(-1)^{(n-1)/2}, \tag{6}$$

where G'_M is dynamic modulus measured at minimum strain, where the instantaneous strain-rates are maximized and G'_L is a large strain dynamic modulus. These measures can be obtained from Fourier coefficients or from numerical differentiation of the material response. In the linear-viscoelastic regime, these measures reduce to first harmonic moduli, $G'_M = G'_L = G'_1(\omega)$. Similarly, the corresponding nonlinear viscous material properties are given as,

$$\eta'_M = \left.\frac{d\sigma}{d\dot{\gamma}}\right|_{\dot{\gamma}=0} = \frac{1}{\omega_n}\sum_{n=odd} nG''_n(-1)^{(n-1)/2}, \tag{7}$$

$$\eta'_L = \left.\frac{\sigma}{\dot{\gamma}}\right|_{\dot{\gamma}=\pm\dot{\gamma}_0} = \frac{1}{\omega_n}\sum_{n=odd} G''_n, \tag{8}$$

where η'_M is dynamic viscosity measured at minimum strain-rate and η'_L is dynamic viscosity measured at maximum strain-rate. From these measures, intra-cycle viscoelastic nonlinearities can also be quantified. The elastic nonlinearity is quantified as strain-stiffening ratio, S, given by,

$$S = \frac{G'_L - G'_M}{G'_L}. \tag{9}$$

The elastic nonlinearity is strain-stiffening for the case when $S > 0$ and is strain-softening when $S < 0$. While the corresponding intra-cycle viscous nonlinearity, quantified as shear-thickening ratio, T, is given by,

$$T = \frac{\eta'_L - \eta'_M}{\eta'_L}. \tag{10}$$

For the case when $T > 0$, the behavior is intra-cycle shear-thinning and shear-thinning when $T < 0$. A detailed description of the nonlinear viscoelastic measures can be found in (Hyun et al. 2011; Ewoldt et al. 2008)

In addition to studying the nonlinearity within an oscillatory cycle (intra-cycle) through the local nonlinear viscoelastic moduli described above, further insights into the origins of the observed nonlinearity can be gained by examining the change in the viscoelastic nonlinear material properties with increasing imposed strain amplitude (inter-cycle) (Ewoldt et al. 2008). Within an oscillatory cycle, the strain and strain rate vary orthogonally. As a result, as the strain is maximized within a cycle, the strain rate goes to zero and vice versa. Thus, the nonlinear viscoelastic response within a given cycle can be affected by the varying strain and/or the varying strain-rate. For the case of elastic nonlinearities, the variation of large-strain modulus, G'_L, with increasing imposed strain amplitude can be attributed to strain-induced nonlinearities since the strain rate at maximum strain is zero. Similarly, the variation of the corresponding minimum-strain modulus, G'_M, with increasing imposed strain-amplitude can be attributed to strain-rate induced nonlinearities as the modulus is evaluated at the point of zero strain within an oscillatory cycle. Thus, changes to G'_L can be thought of as strain softening or strain hardening while changes to G'_M can be thought of as strain-rate softening or strain-rate hardening. By comparing the relative magnitude of G'_M and G'_L, as a function of strain amplitude, one can infer whether the observed nonlinearities are dominated by changes in strain or strain rate within an oscillation cycle. As a consequence, when the magnitude of $G'_M >> G'_L$, we will designate the nonlinear response of the fluid to be strain-rate hardening/softening while if the magnitude $G'_M << G'_L$ we will designate the fluid's nonlinear response to be strain hardening/softening. In a similar manner, the dependence of the viscous nonlinearity on the amplitude of the imposed strain or strain-rate within an oscillatory cycle can be studied by examining the inter-cycle variation of the local nonlinear dynamic viscosity measures, η'_M and η'_L. As before, since η'_L is evaluated at the maximum strain rate and η'_M is evaluated when the strain rate is zero and the strain is maximized, changes to η'_L can be thought of as strain-rate thinning or strain-rate thickening, while changes to η'_M can be thought of as strain thinning or strain thickening. If the magnitude of $\eta'_L >> \eta'_M$, then the viscous nonlinearities can be considered dominated by strain-rate thickening/thinning effect while if the magnitude

of $\eta'_L << \eta'_M$ then the viscous nonlinearities can be thought of as dominated by strain thickening/thinning effects.

Experimental

Materials

Hydrophilic fumed silica (AEROSIL @ 200) with specific surface area of 200 m^2/g and primary particle size 12 nm was graciously supplied by Degussa. Polyethylene oxide (PEO) with a molecular weight of M_w = 600 kg/mol was purchased from Aldrich Chemicals. A fumed silica in PEO dispersion ($FLOC$) was prepared according to (Khandavalli and Rothstein 2014). A fumed silica dispersion in polypropylene glycol (M_w = 1000 g/mol, Aldrich Chemicals) ($HydroC$) was prepared according to Chellamuthu et al. (2009). Cornstarch was purchased from a local grocery store and the cornstarch suspension in water (JAM) was prepared according to Bischoff White et al. (2010).

Shear rheometry

Shear rheology was conducted on a stress-controlled TA DHR-3 rheometers using a 40 mm 2° aluminum cone-plate geometry at a constant temperature of 23 °C temperature. A solvent trap was used to prevent sample evaporation during measurements. The samples were pre-sheared before conducting any rheological measurements to erase any shear history during sampling preparation and handing and allowed to rest for few minutes to reach equilibrium (Raghavan and Khan 1995; Galindo-Rosales and Rubio-Hernàndez 2010; Khandavalli and Rothstein 2014). Steady shear rheological measurements were conducted in the shear rate range of 0.01 to 100 s^{-1}. The small amplitude oscillatory shear tests were conducted in the frequency range 1 to 100 rad/s, with a fixed strain amplitude chosen to place the measurements well within the LVE region. The large amplitude oscillatory shear measurements were conducted for strain amplitude range between 0.01 and 1000 % for different frequencies between 3 and 30 rad/s. The high frequencies were used to insure that the solutions were probed at shear rates where shear thickening was observed in the steady shear measurements. A sufficient number of oscillatory cycles were run, ranging from 30 to 80, to ensure a steady-state measurement. The nonlinear viscoelastic material parameters such as, the Lissajous-Bowditch plots and the nonlinear viscoelastic parameters such as minimum/maximum-strain dynamic moduli and minimum/maximum-rate dynamic viscosity, were obtained using the Fourier-transform software application of the TA DHR-3 rheometer. The FT-Rheology application processes the raw torque signal and the extracts nonlinear parameters from the reconstructed/filtered signal. The reconstructed stress signal was double checked with the steady raw stress signal to check for poor reconstruction of any noisy signal. The data points affected by noise or inaccurate analysis of the TRIOS software were either excluded from the manuscript or the nonlinear viscoelastic parameters were recalculated from the Lissajous-Bowditch plots. As the LAOS measurements were performed on a stress controlled rheometer, the data can be affected by inertia (Merger and Wilhelm 2014). An oscillatory mapping of the geometry was performed to compensate for the influence of instrument inertia. However, when the torque generated by instrument inertia is large, the rheometer's compensation routines are not sufficient to completely eliminate the effect of instrument inertia. To insure high quality data, the relative ratio of inertia torque to sample torque, $T_{inertia}/T_{sample}$, was checked for each experimental data point. When the ratio of inertial torque to sample torque was greater than 20 %, $T_{inertia}/T_{sample} > 20\,\%$, the data were discarded. Merger and Wilhelm (2014) demonstrated that, beyond a ratio of 20 %, the sample response is affected by instrument inertia. However, below a ratio of 20 %, quantitative agreement between measurements on strain controlled and stress controlled rheometers can be achieved. Any experimental artifacts such as wall slip and edge fracture in measurements are identified by examining the presence of even harmonic intensity which are sensitive to asymmetric artifacts (Graham 1995). For all cases, the magnitude of even harmonics was found to be very small. For $FLOC$ and $HydroC$ dispersions, the intensity of even harmonics relative to the fundamental (I_2/I_1) was found to be less than 1 % and for JAM the even harmonics (I_2/I_1) were found to be less than 7 %. All LAOS measurements were repeated several times to ensure consistency in the trends and are reproducible.

Results and discussion

Here, we present a nonlinear viscoelasticity investigation of three particle dispersions which shear-thicken by three different mechanisms. The first material system is fumed silica nanoparticles (4.5 wt.%) dispersed in aqueous PEO (0.4 wt.%) of M_w = 600 kg/mol ($FLOC$). This system shear-thickens due to shear-induced formation of large particle clusters flocculated by polymer bridging (Khandavalli and Rothstein 2014; Kamibayashi et al. 2008). The second system is fumed silica nanoparticles (20 wt.%) dispersed in polypropylene glycol ($HydroC$). Shear-thickening in this system occurs due to the formation of hydroclusters where the lubrication hydrodynamic forces play an important role in shear-thickening (Wagner and Brady 2009; Chellamuthu et al. 2009). The third system is a dense

suspension of cornstarch in water (56 wt.%) (JAM). This system shear-thickens by jamming mechanism, where the frictional/contact forces of the jammed particle clusters are responsible for the increase in viscosity (Fall et al. 2010; Brown and Jaeger 2009). The shear-thickening mechanisms of the three systems will be discussed in more detailed in the next section. The three systems are labeled based on their shear-thickening mechanisms to make the interpretations easier. The objective of this study is to identify the viscoelastic nonlinearities associated with each mechanisms and compare/contrast between the three mechanisms. Prior to studying LAOS behavior, steady-shear and small amplitude oscillatory shear rheology behavior will be presented.

Steady shear rheology

The steady-shear rheology of three particle dispersions, $FLOC$, $HydroC$, and JAM, are shown in Fig. 1. The three dispersions exhibited shear-thickening by more than an order of magnitude at imposed shear rates between 2 s^{-1} and 10 s^{-1}. The different mechanisms by which the three dispersions shear thicken have been well studied in literature. For the case of $FLOC$ colloidal dispersion, the higher molecular weight PEO polymer has a strong affinity for adsorption onto the fumed silica surface through hydrogen bonded interactions (Voronin et al. 2004). Under shear flow, the free ends of polymer chains adsorbed onto particles at equilibrium can adsorb onto more neighboring particles and can create a larger particle clusters bridged by polymer chains. Beyond a critical shear-rate, the increase in the cluster formation due to bridging of more particles by polymer chains induced by shear fields, results in a strong increase in the viscosity and the observed shear-thickening (Kamibayashi et al. 2008; Khandavalli and Rothstein 2014; Otsubo 2001). The second system, $HydroC$ colloidal dispersion, shear-thickens by hydrocluster mechanism (Wagner and Brady 2009). At very low Peclet number, $Pe = a^2\ \dot{\gamma}/D_0$, the microstructure relaxes through Brownian mechanism. Here, D_0 is the diffusion coefficient of the particles in solution and a is the particle size. As the Peclet number is increased, the hydrodynamic forces begin to compete with the Brownian forces. Beyond a critical increase in Peclet number, when the hydrodynamic forces predominate over the Brownian forces, can result in the formation of large anisotropic hydroclusters. These hydroclusters are associated with large lubrication hydrodynamic forces and cause shear-thickening (Wagner and Brady 2009; Raghavan and Khan 1997; Chellamuthu et al. 2009). For the case of JAM, a dense non-Brownian suspension, the shear-thickening behavior is due to dilatancy and eventual jamming (Fall et al. 2008, 2010; Brown and Jaeger 2009; Bertrand et al. 2002). Due to confinement of the particles within boundaries and crowding at high volume fractions, the particles jam into the neighboring particles in order to accommodate the imposed flow. The resulting large stresses associated with the frictional forces due to particle contacts when jammed are the cause for shear-thickening (Fall et al. 2008, 2010; Brown and Jaeger 2009).

Small amplitude oscillatory shear rheology (SAOS)

The SAOS behavior is compared between the three shear-thickening dispersions in Fig. 2. The $FLOC$ exhibited a gel-like response, where the storage modulus, G'_1, and loss modulus, G''_1, were approximately independent of frequency. The predominantly elastic response is likely the result of gel-like microstructure at equilibrium resulting from the hydrogen bonded interactions between PEO polymer and silica groups of nanoparticles (Khandavalli and Rothstein 2014; Otsubo 1993). The $HydroC$ dispersion, in contrast to $FLOC$, exhibited predominantly viscous-like

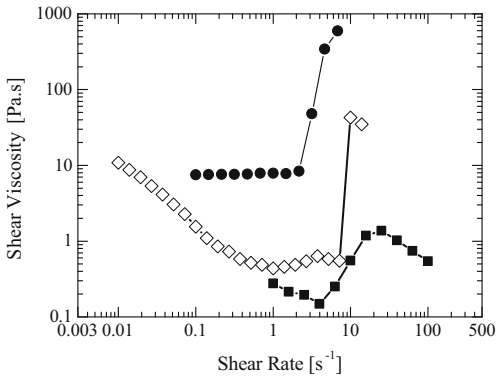

Fig. 1 Steady shear viscosity as a function of shear rate for a series dispersions of (*black square*) $FLOC$, (*black circle*) $HydroC$, and (*white diamond*) JAM

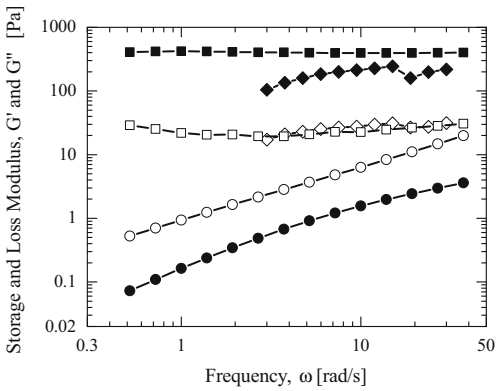

Fig. 2 Linear viscoelastic measurements of the storage modulus (*filled symbols*) and loss modulus (*hollow symbols*) as a function of angular frequency for a series of dispersions of (*black square*) $FLOC$, (*black circle*) $HydroC$, and (*black lozenge*) JAM

behavior, where the loss modulus was consistently larger than the elastic modulus, $G_1'' > G_1'$, in the frequency range tested. Both the elastic and loss modulus scale approximately with a similar power law with frequency. These observations were consistent with the literature (Raghavan et al. 2000). The JAM suspension exhibited approximately a frequency independent behavior, with $G_1' > G_1''$ indicating predominantly elastic behavior. At low concentrations, the microstructure formed in particle dispersions typically relax through Brownian motion at equilibrium (Larson 1999). However, because of the high particle volume fraction in the cornstarch-water ($\phi = 0.45$), the relaxation time scales increase as the diffusivity of the particle is reduced, $\tau \sim D_0^{-1}$, due to increased confinement between neighboring particles. The result is an increased elasticity as observed in Fig. 2 and seen in the literature (Larson 1999; Mason and Weitz 1995).

Large amplitude oscillatory shear rheology (LAOS)

Fumed silica in PEO ($FLOC$)

The large amplitude oscillatory shear behavior of fumed silica in PEO ($FLOC$) at different frequencies ranging from 10 to 30 rad/s is shown in Fig. 3. The angular frequencies were chosen to ensure that the nonlinear response of the fluid would be well into the shear-thickening regime observed in Fig. 1. The storage, G_1', and loss modulus, G_1'', were found to be independent of percent strain until about 2 or 3 % strain, indicating LVE behavior below that point. The storage modulus was approximately two orders of magnitude larger than the loss modulus indicating predominantly elastic behavior which is consistent with small amplitude oscillatory shear behavior shown in Fig. 2. Beyond the LVE limit, the elastic modulus was observed to decline with increasing strain, whereas the loss modulus exhibited a weak overshoot before declining at large strains. Such plastic nonlinear behavior at large amplitudes is typical of weak colloidal gels (Sun et al. 2011) even those that are shear-thinning. The first-harmonic moduli response does not appear to be universal for colloidal systems flocculated by polymer bridging, some of those systems which shear-thicken in steady-shear by the same shear-induced bridging mechanism have been shown to possess an increased G_1' and G_1'' in the nonlinear region (Otsubo 1999). The likely cause for the differences in response will be discussed in the later sections. The LAOS response for different frequencies showed no significant quantitative or qualitative differences in the trends in G_1' and G_1'' behavior with increasing strain amplitude.

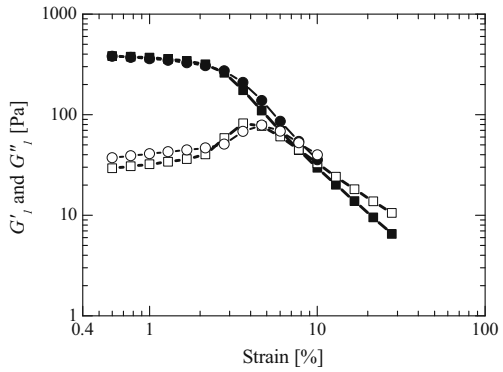

Fig. 3 Storage modulus (*filled symbols*) and loss modulus (*hollow symbols*) as a function of strain amplitude for $FLOC$. The data include experiments at several frequencies of (*black square*) 10 rad/s and (*black circle*) 30 rad/s

In the nonlinear viscoelastic region, higher harmonic stresses arise (Wilhelm et al. 1998). Although the dominant response was found to be from the first harmonic, additional insights can be gained from the response due to higher harmonics contribution. The nonlinear response of $FLOC$ can be visualized graphically from the elastic Lissajous-Bowditch plots. These plots of stress versus strain are presented in Fig. 4. As expected, in the LVE limit at small strains, the resulting elastic Lissajous-Bowditch plots were found to be straight lines. In the nonlinear regime, the plots become distorted due to the contribution of higher order harmonics. The nonlinearities of $FLOC$ were further examined through the local viscoelastic material properties quantified within an oscillatory cycle. The minimum-strain dynamic moduli, G_M', and large-strain dynamic moduli, G_L', are shown in Fig. 5a as a function of strain amplitude. In the LVE region, these measures reduce to first-harmonic storage modulus as expected. In the nonlinear region, both G_M' and G_L' were found to decrease with increasing strain amplitude for all frequencies, indicating a softening behavior with both increasing imposed strain and strain rate within an oscillatory cycle. The minimum-strain (maximum-strain rate) modulus, G_M', was found to decrease more quickly than the large-strain (minimum-strain rate) modulus, G_L', with increasing strain amplitude. This suggests that the elastic nonlinearity of $FLOC$ is dominated by strain-rate-softening of the elastic modulus. The strain-rate-softening behavior is likely due to alignment of the microstructure to the flow fields.

The elastic nonlinearities were further examined through the measure, stiffening ratio, S, plotted as a function of applied strain amplitude in Fig. 7a. In the LVE limits, where the elastic Lissajous-Bowditch plots look straight lines, the stiffening ratio is $S \sim 0$ as expected. As described in the theoretical background section, the stiffening ratio given by Eq. 9 describes whether the elastic modulus softens, $S < 0$, or stiffens, $S > 0$, with increasing strain within an oscillatory cycle. In the nonlinear region, beyond a strain of 4 %, the LAOS behavior of the $FLOC$ within an oscillatory

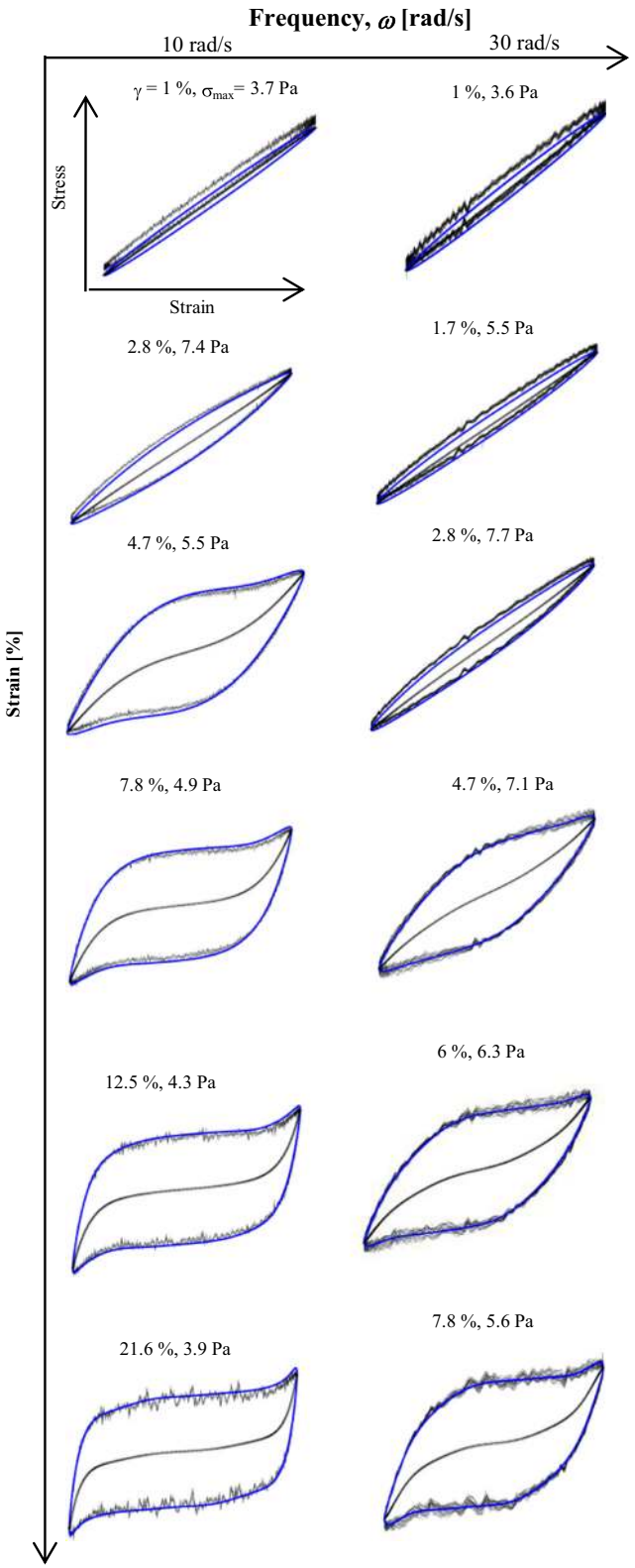

Fig. 4 Elastic Lissajous-Bowditch plots, (*blue*) total stress and (*black*) elastic versus strain, for $FLOC$ dispersion for several different strain amplitude and frequency. The raw waveforms are also co-plotted in *black lines*

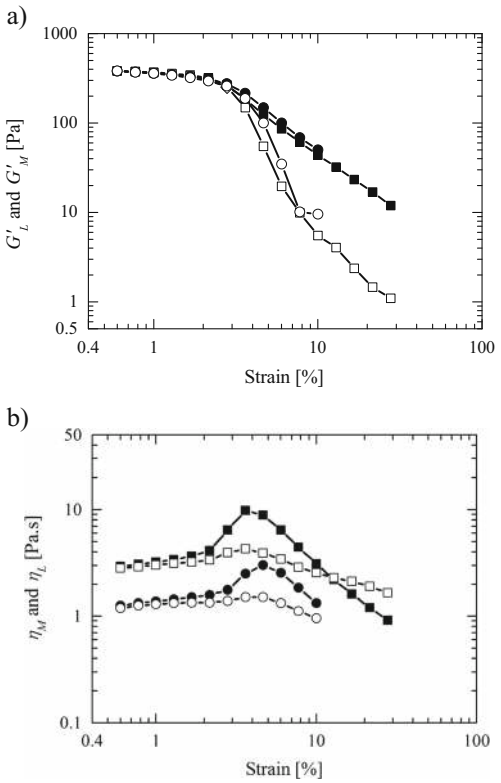

Fig. 5 Nonlinear viscoelastic measures **a** G'_L (*filled symbols*), G'_M (*hollow symbols*) and **b** η'_L (*filled symbols*), η'_M (*hollow symbols*) as a function of strain amplitude for $FLOC$. The data include experiments at frequencies of (*black square*) 10 rad/s and (*black circle*) 30 rad/s

cycle was found to be strain-stiffening, $S > 0$. This can be observed in the elastic Lissajous-Bowditch plot as a sharp upturn in the stress at large strains. However, the behavior is in contrast to the large-strain dynamic moduli, G'_L, which was found to soften with increasing imposed strain amplitude. This discrepancy is the result of the definition of the stiffening ratio and can lead to misinterpretation of the results. The stiffening ratio can be greater than zero, $S > 0$, if the large strain modulus, G'_L, stiffens more quickly than the minimum strain modulus, G'_M, or if G'_M softens more quickly than G'_L. Thus, $S > 0$ can be interpreted as either strain-hardening or strain-rate softening of the material and only through examination of G'_L and G'_M can the distinction be made and the interpretation of the data be valid.

As described above, In an oscillatory cycle, the strain and strain-rate vary orthogonally. As a result, within an oscillatory cycle, the strain rate goes to zero as the strain is maximized and vice versa. The elastic stress response within a given cycle can thus be affected by either the varying strain and/or the varying strain-rate. For the case of $FLOC$, based on the measurements of G'_L and G'_M, the dominant nonlinearity within the cycle is a softening with increasing strain rate. Therefore, the nonlinearity of $FLOC$ within a cycle

can be interpreted as strain-rate-softening rather than strain stiffening.

Similarly, the corresponding viscous nonlinearities can be examined graphically from viscous Lissajous-Bowditch plots. These stress versus strain-rate plots are presented in the Fig. 6. The viscous nonlinearity quantified through the measures, minimum strain-rate dynamic viscosity, η'_M, and the large strain-rate dynamic viscosity, η'_L, are also shown in Fig. 5b. Both the measures showed mild thickening behavior at medium strain amplitudes and thinning behavior at large strain amplitudes. However, the nonlinearity of η'_L was found to be stronger than η'_M suggesting predominant strain-rate thickening at moderates strains followed by a strain-rate thinning behaviors with increasing strain amplitude.

The viscous nonlinearities are quantified using the shear-thickening ratio, T, and are presented in Fig. 7b. As described in the theoretical background section, the shear-thickening ratio given by Eq. 10 describes whether the viscosity thins, $T < 0$, or thickens, $T > 0$, with increasing strain rate. The shear thickening ratio of the $FLOC$ was found to exhibit the same shear-thickening and shear-thinning behavior with increasing strain amplitude as η'_M and η'_L. The shear-thickening behavior of the $FLOC$ at medium strain amplitudes is commonly attributed to the transients present at the start-up for colloidal systems (Sun et al. 2011). Such behavior could be related to the break down of gel-like microstructure built up at equilibrium/rest as has been observed in steady shear (Wagner and Brady 2009; Kawaguchi et al. 1996). The strain-rate thinning at large strain amplitudes could be due to orientation or yielding of microstructure to the flow fields (Kamibayashi et al. 2008; Kawaguchi et al. 1996).

If the viscous nonlinearities of the $FLOC$ observed through LAOS are compared with the steady-shear measurements in Fig. 1, a shear thickening of the viscosity is expected for shear rates between 4 and 20 s^{-1}. However, as seen in Figs. 5b, 6 and 7b, this is clearly not the case. The inconsistency between the steady shear and LAOS measurements indicates a sensitivity of the associated shear-thickening mechanism to the instantaneous shear rates and strains imposed during the oscillatory cycle. Unlike steady-state deformation, the shear rates are not constant throughout a LAOS experiment. This can be demonstrated with a simple stress growth experiment. In Fig. 8, viscosity is plotted against accumulated strain for our three fluids at a constant shear rate. At shear rates where shear thickening occurs, the viscosity of $FLOC$ grows to a steady-state value only after a significant amount of strain is accumulated. This suggests that a minimum strain, in addition to a minimum shear rate, is necessary for shear thickening by the associated mechanism for these nanoparticle-polymer systems. In fact, the strains needed to achieve shear thickening for the $HydroC$ are so large, $\gamma > 100{,}000$ %, that they cannot be

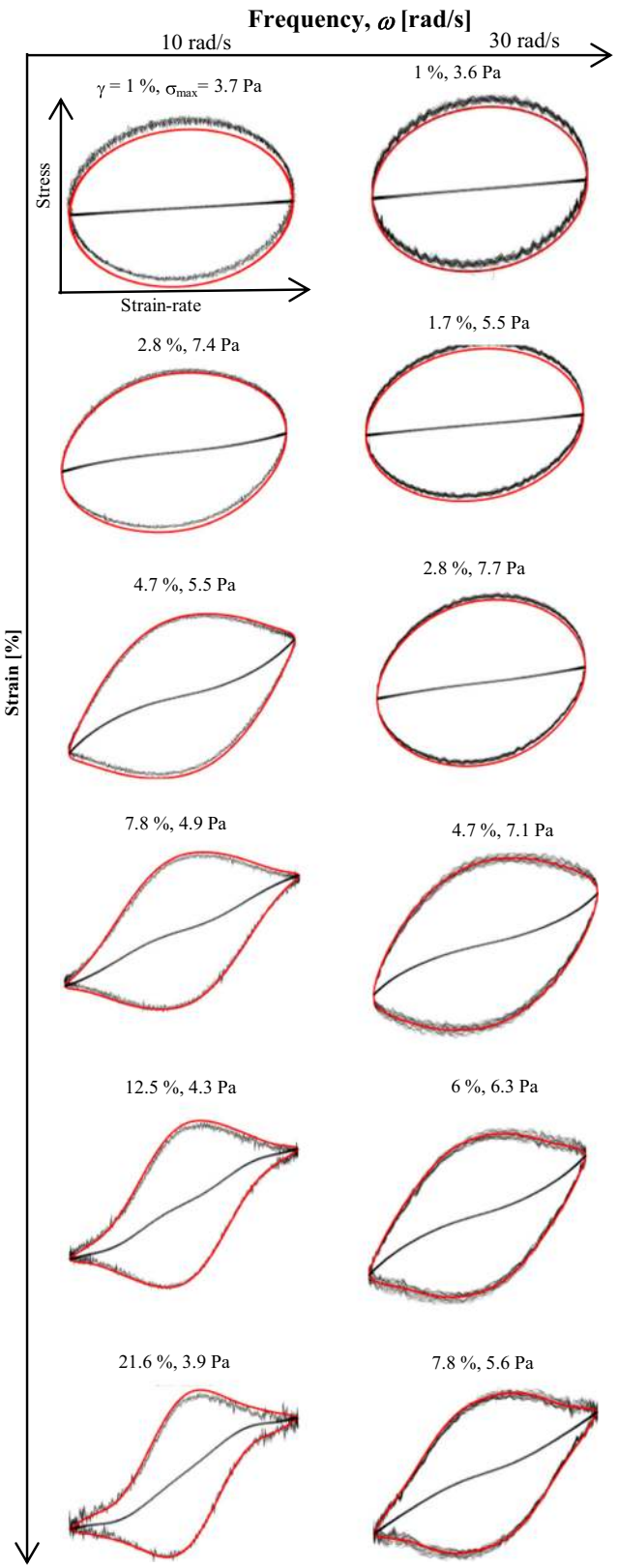

Fig. 6 Viscous Lissajous-Bowditch plots, (*red*) total stress and (*black*) viscous versus strain, for $FLOC$ dispersion for several different strain amplitude and frequency. The raw waveforms are shown in *black lines*

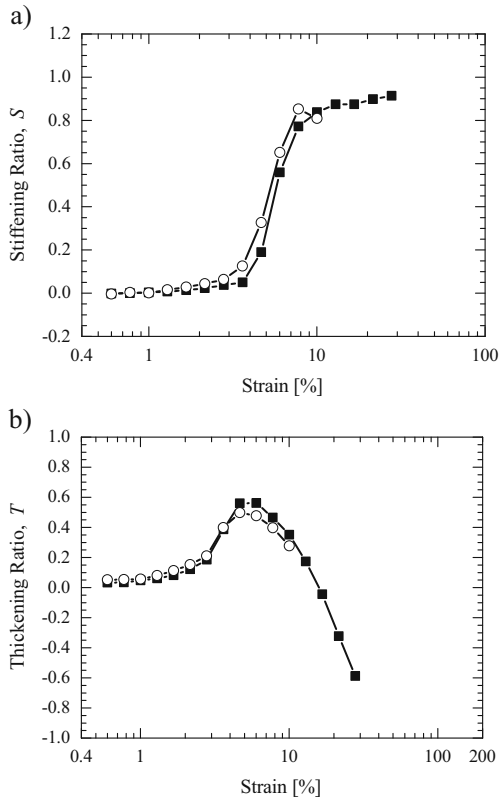

Fig. 7 **a** Stiffening ratio and **b** thickening ratio as a function of strain amplitude for $FLOC$. The data include experiments at frequencies of (*black square*) 10 rad/s and (*black circle*) 30 rad/s

achieved in LAOS. At smaller strains, the steady-shear viscosity of $FLOC$ solution thins with increased strain. By comparison, the strains needed to induce shear-thickening for both the $HydroC$ or JAM are two or three orders of magnitude smaller and easily obtainable in LAOS. Interestingly, the first-harmonic moduli for some colloidal systems flocculated by polymer bridging which also shear thicken in steady shear by the same shear-induced bridging mechanism show a contrasting increase in both the elastic and viscous modulus in the nonlinear deformation range (Otsubo 1999). These differing observations could be due to the difference in the critical strains associated with each material system required for shear thickening to occur; however, the experiments of Otsubo do not contain the start up data needed to make this hypothesis conclusive.

To summarize the LAOS behavior of $FLOC$, the system exhibited both strain softening and strain-rate softening of the elastic nonlinearity. The strain-rate softening behavior appeared to be dominant over strain-softening response resulting in a positive stiffening ratio. The strain-rate softening behavior is likely due to yielding or break down of the microstructure. The viscous nonlinearity exhibited mild strain-rate thickening at medium strain rates which could

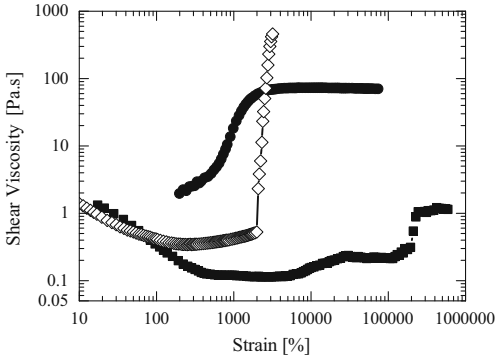

Fig. 8 Viscosity evolution under fixed shear rate for shear-thickening dispersions of (*black square*) $FLOC$ at a shear rate of $\dot{\gamma} = 20\,\mathrm{s}^{-1}$, (*black circle*) $HydroC$ at $\dot{\gamma} = 7\,\mathrm{s}^{-1}$ and (*white diamond*) JAM (53 % Cornstarch in water) at $\dot{\gamma} = 15\,\mathrm{s}^{-1}$

be due to dissipation of the equilibrium gel like microstructure. At large strain amplitudes, the behavior evolved to strain-rate thinning associated with microstructure yielding. In comparison to steady-shear, shear-thickening behavior by shear-induced mechanism was not observed in large amplitude oscillatory. The stress growth measurements indicated that very large strain amplitudes are required for shear-thickening to occur by such mechanism too large in fact to be achieved in LAOS.

Fumed silica in PPG (HydroC)

The amplitude sweeps of the solution of fumed silica in PPG ($HydroC$) for angular frequencies ranging from 3 to 30 rad/s are shown in Fig. 9. In the LVE region, the loss modulus was found to be greater than that of the storage modulus, $G_1'' > G_1'$, which indicates a predominantly viscous behavior. With increasing strain amplitude, both G' and G" initially showed strain softening/strain-rate thinning behavior. This behavior became weaker as

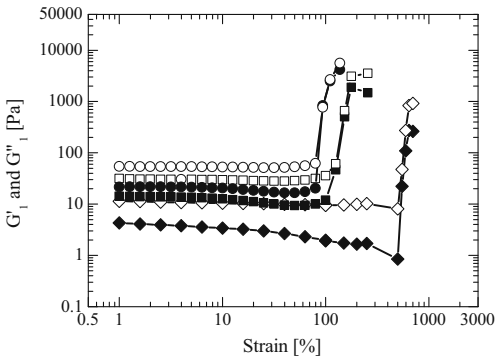

Fig. 9 Storage modulus (*filled symbols*) and loss modulus (*hollow symbols*) as a function of strain amplitude for $HydroC$. The data include experiments at several frequencies of (*white diamond*) 3 rad/s and (*black square*) 10 rad/s and (*white circle*) 30 rad/s

the frequency was increased. The strain softening/strain-rate thinning behavior could be due to alignment of the microstructure to the flow fields, similar to the shear-thinning regime observed in steady-shear behavior shown in Fig. 1. Beyond a critical strain amplitude, both G_1' and G_1'' were found to be dramatically increase by more than an order of magnitude with increasing strain indicating both a strong strain-stiffening and a strong strain-rate thickening behavior (Raghavan and Khan 1997; Chellamuthu et al. 2009). The critical strain required for the onset of strain-stiffening/thickening was seen to decrease with increasing angular frequency. This is likely due to an increasing Peclet number with increasing frequency and increased importance of the imposed flow stresses compared to diffusion.

The elastic non-linearity of $HydroC$ can be examined through the elastic Lissajous-Bowditch plots shown in Fig. 10. The corresponding quantified non-linear elastic measures, the minimum-strain dynamic moduli, G_M', and the large-strain dynamic moduli, G_L' are shown in Fig. 11a. At small strain amplitudes, the magnitudes of G_M' and G_L' were approximately equal indicating little non-linearity. Beyond a critical strain amplitude, both the G_M' and G_L' were found to increase dramatically with strain amplitude.

This indicates a strong strain-stiffening and strain-rate-stiffening behavior similar to what was observed for the first-harmonic of the elastic moduli. Throughout the stiffening region, the magnitude of G_M' was found to be slightly larger than that of G_L'. This stiffening within an oscillatory cycle can be observed graphically from the distorted elastic Lissajous-Bowditch plots shown in Fig. 10 and result in softening of the stiffening ratio, $S < 0$, at large imposed strain amplitudes. As before, this result can be misinterpreted because it is not due to the softening of the moduli within a cycle, but the more rapid stiffening of the minimum strain (maximum strain rate) modulus, G_M', compared to the large strain modulus, G_L', as seen in Fig. 11a. This is another example where the stiffening ratio can mask some of the details in the underlying nonlinear rheology when an elastic response is dominated by nonlinearities associated with increasing strain-rates. The appropriate interpretation thus is that the elastic nonlinearities of $HydroC$ are strain-rate stiffening.

The viscous nonlinearities can be graphically visualized through viscous Lissajous-Bowditch plots shown in Fig. 12. The nonlinear quantities, minimum strain-rate dynamic viscosity, η_M', and large strain-rate dynamic viscosity, η_L', were also presented in Fig. 11b. Like the elastic nonlinearities for $HydroC$, both η_M' and η_L' increase dramatically beyond a critical oscillatory strain amplitude. This is indicative of strain thickening and strain-rate thickening behavior mirroring the response of the first-harmonic of loss modulus.

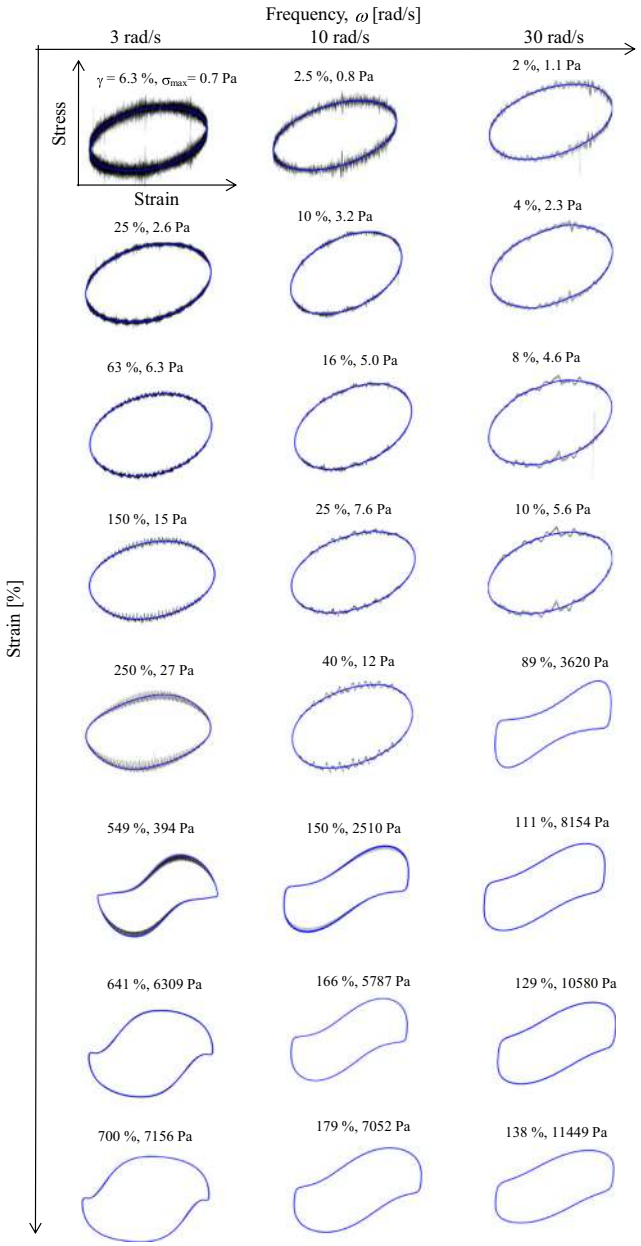

Fig. 10 Elastic Lissajous-Bowditch plots, total stress versus strain, for $HydroC$ dispersion for several different strain amplitude and frequency. The raw waveforms are shown in black line

The details of nonlinearities of $HydroC$ within an oscillatory cycle were also investigated through the thickening ratios shown in Fig. 13b. For the $\omega = 3$ rad/s frequency case, in the thickening region, the maximum shear-rate dynamic viscosity, η_L', was found to be consistently larger than the minimum shear-rate dynamic viscosity, η_M', resulting in a positive thickening ratio, $T > 0$. This behavior is consistent with the variations in the loss modulus observed in Fig. 9. While for the larger frequency tested, $\omega > 3$ rad/s, η_M' was found to be consistently larger than that of η_L', resulting in a thinning of the thickening ratio, $T < 0$.

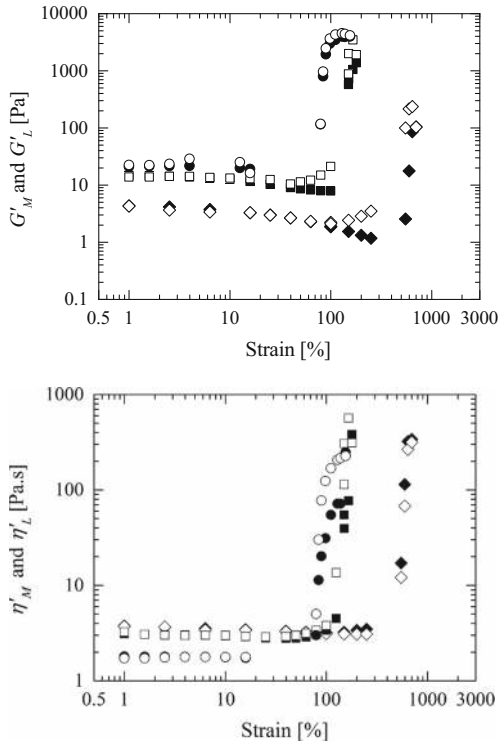

Fig. 11 Nonlinear viscoelastic measures **a** G'_L (*filled symbols*), G'_M (*hollow symbols*) and **b** η'_L (*filled symbols*), η'_M (*hollow symbols*) as function of strain amplitude for $HydroC$. The data include experiments at several frequencies of (*white diamond*) 3 rad/s, (*black square*) 10 rad/s, and (*white circle*) 30 rad/s

This suggests that the appearance of shear-thinning in the Lissajous-Bowditch plots is predominantly due to strain-induced thickening of η'_M within the cycle. At these high frequencies, the shear rates through out most of the cycle is likely sufficient to induce hydrocluster formation and as a result with increasing strain more hydroclusters are formed and the fluid becomes more viscous.

To summarize, the $HydroC$ at large strain amplitudes exhibited strong strain-stiffening and strain-rate stiffening nonlinearities associated with hydrocluster mechanism. By comparison, however, the magnitude of the stiffening driven by the increasing large imposed strain-rates within a cycle was found to be more significant than the nonlinearities induced by increasing the strain amplitudes within an oscillatory cycle. The corresponding viscous non-linearities showed strong strain-thickening and strain-rate thickening behavior at large strain amplitudes. However, the thickening behavior was found to depend on frequency. For low frequencies, $\omega = 3$ rad/s, the thickening was dominated by nonlinearities associated with the behavior at strain-rates. While at high frequencies, $\omega > 3$ rad/s, the thickening of the viscosity was dominated by large-strain-induced nonlinearities and was less sensitive to increasing strain rates within an oscillatory cycle.

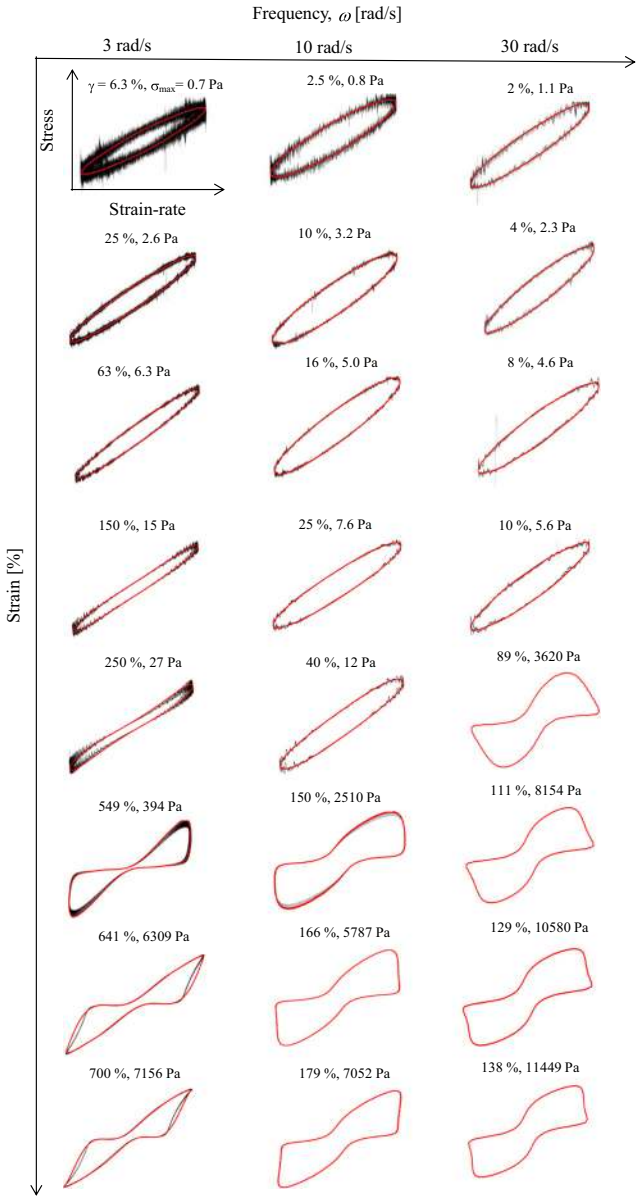

Fig. 12 Viscous Lissajous-Bowditch plots, total stress versus strain-rate, for $HydroC$ dispersion for several different strain amplitude and frequency. The raw waveforms (black line) are co-plotted along with the reconstructed data

Cornstarch in water (JAM)

The amplitude sweep of cornstarch in water (JAM) at 10 rad/s frequency is shown in Fig. 14. Unfortunately, the study at a wider frequency range was not possible due to experimental difficulties. At small strain amplitudes, the storage modulus was found to be larger than the loss modulus, $G'_1 > G''_1$, indicating a predominantly elastic behavior. With increasing strain amplitude, the moduli initially declined, indicating a strain softening/strain-rate thinning behavior. This behavior is likely due to the alignment of particles to

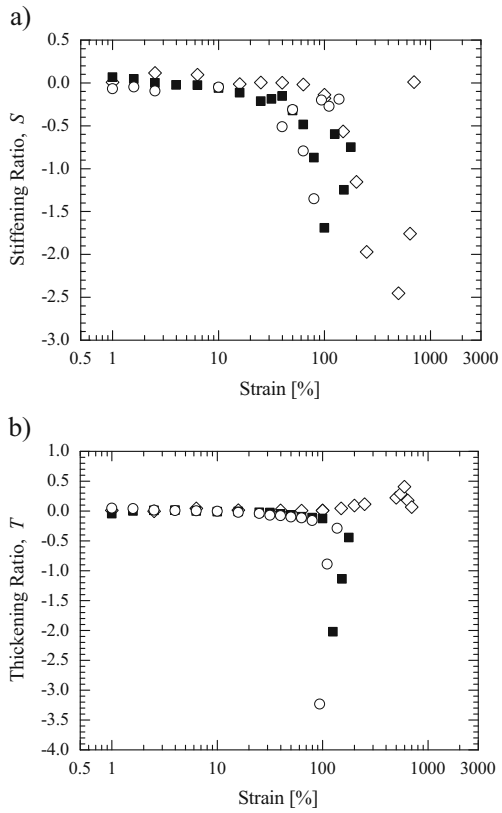

Fig. 13 **a** Stiffening ratio and **b** thickening ratio as a function of strain function of strain amplitude for $HydroC$. The data include experiments at several frequencies of (*white diamond*) 3 rad/s, (*black square*) 10 rad/s, and (*white circle*) 30 rad/s

the shear-fields, similar to shear-thinning regime in steady-shear rheology shown in Fig. 1. Note that in Fig. 14, data points appear to be missing at moderate strains of 3 and 80 %. Using the protocol described in the experimental section, the data within this range was found to affected by instrument inertia and was removed. This was caused primarily by shear thinning of the fluid viscosity and the resulting reduction of the viscous stresses. At larger strains,

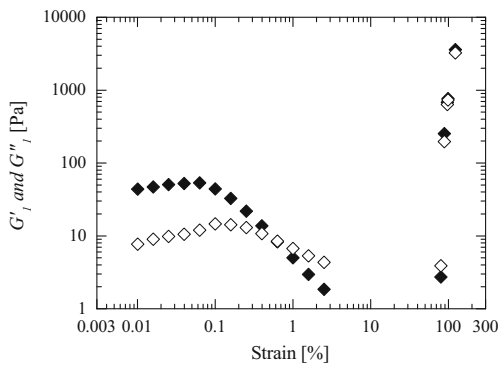

Fig. 14 Storage modulus (*filled symbols*) and loss modulus (*hollow symbols*) as a function of strain amplitude at 10 rad/s for JAM

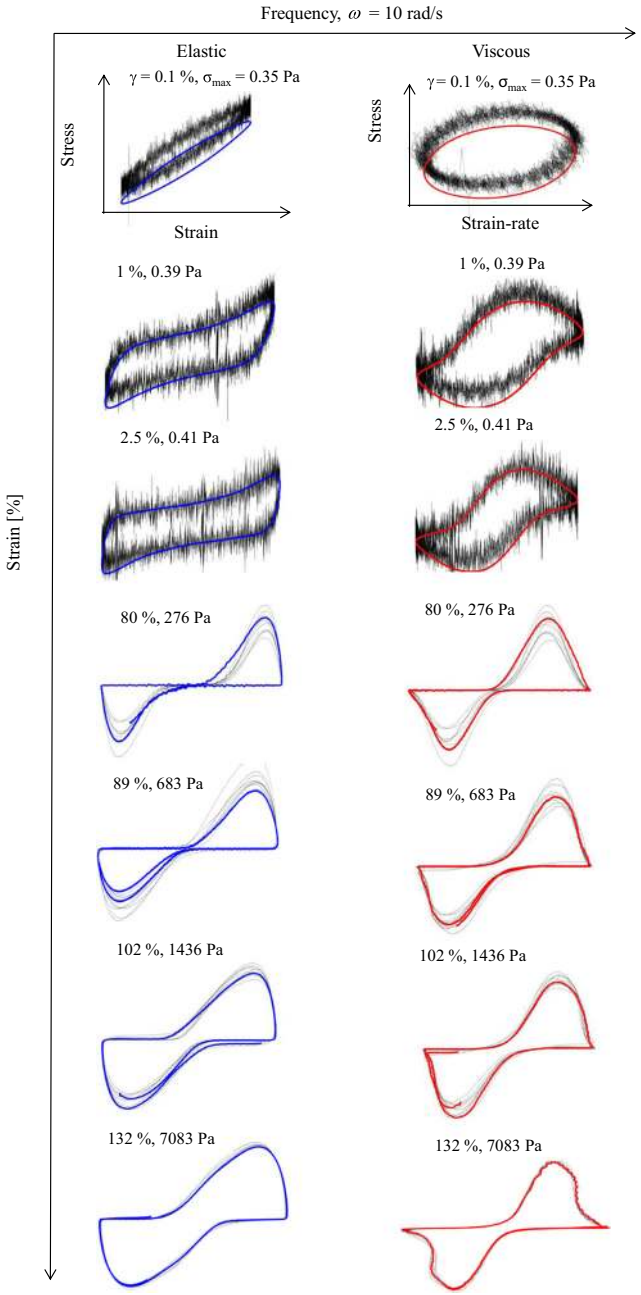

Fig. 15 Elastic (*blue*) and viscous (*red*) Lissajous-Bowditch plots, total stress vs. strain/strain-rate for JAM suspension for several different strain amplitude at 10 rad/s. The raw waveforms (*black line*) are co-plotted along with the reconstructed data

the onset of shear thickening increased the shear stress by more than an order of magnitude. As a result, at these larger strains, the inertial contribution to the measured torque again fell below the 20 % threshold and the data were included. At large strains, both storage and loss moduli showed strong strain stiffening/strain-rate thickening behavior. The mechanism for the stiffening/thickening behavior appears to be similar to jamming that has been observed

in steady-shear measurements. Such stiffening of elastic modulus has also been reported for dense non-colloidal suspensions and has been attributed to shear-induced migration of particles (Nam et al. 2011).

The elastic non-linearities of JAM can be visualized through the Lissajous-Bowditch plots are presented in Fig. 15. The nonlineartiy was examined through the measurements of minimum-strain dynamic modulus, G'_M, and the large-strain dynamic modulus, G'_L, as a function of an applied strain as shown in Fig. 16a. At low strain, the moduli were both found to soften with increasing strain amplitude. At the largest strains tested, this behavior was found to reverse itself and a strain stiffening and a strain-rate stiffening of the moduli was observed. The critical strain for the transition from softening to stiffening was similar to that observed for the first harmonic storage modulus. In the softening region, the minimum-strain dynamic modulus, G'_M, was found to decrease slightly faster than the large strain-dynamic modulus, G'_L. While in the stiffening region, the G'_M was observed to grow much more quickly than G'_L. This behavior suggests that the elastic non-linearities are predominantly driven by the increasing strain-rates.

To further illustrate the elastic nonlinearities observed within a given oscillatory cycle, the stiffening ratio is shown in Fig. 17. As we have seen a number of times already, the

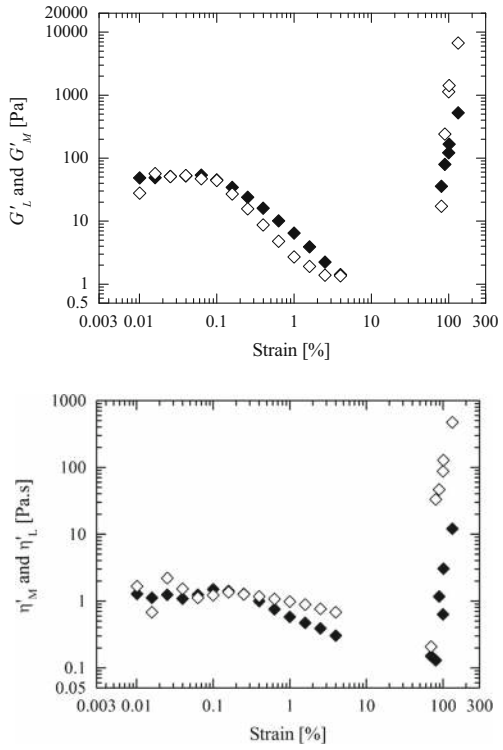

Fig. 16 Nonlinear viscoelastic measures **a** G'_L (*filled symbols*), G'_M (*hollow symbols*) and **b** η'_L (*filled symbols*), η'_M (*hollow symbols*) as a function of strain amplitude for JAM

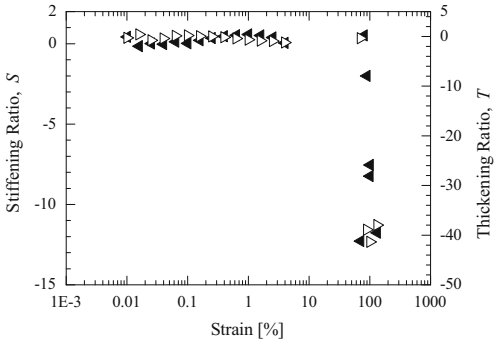

Fig. 17 (*black triangle left*) Stiffening ratio and (*white triangle right*) thickening ratio as a function of strain amplitude at 10 rad/s for JAM suspension

stiffening ratio is misleading. At intermediate strains, the stiffening ratio was found to be strain-stiffening, $S > 0$, not because the moduli are increasing, but because the minimum strain (maximum strain rate) modulus decreases faster than the large strain modulus. Additionally, at large strains, the stiffening ratio appears to be strain-softening, $S < 0$. As a result, the appropriate interpretations of the nonlinearities occurring within an oscillatory cycle is that at moderate strain amplitudes the elastic nonlinearities of the JAM system were strain-rate softening and at large applied strain amplitudes the elastic nonlinearities transition to a strain-rate stiffening behavior as the particles begin to interact and suspension begins to jam.

The viscous nonlinearity of JAM can be visualized through Lissajous-Bowditch plots in Fig. 15. The nonlinearities were quantified through the local measurements of minimum strain-rate dynamic viscosity, η'_M, and the large strain-rate dynamic viscosity, η'_L, as shown in Fig. 16b. Both the viscosities initially exhibited strain/strain-rate thinning behavior at small strains. At large strain amplitudes, this behavior reversed itself becoming strain/strain-rate thickening. This behavior is quite similar to observations of first-harmonic loss modulus. The strain-thickening was found to be as much as two orders of magnitude stronger than the strain-rate thickening. This observation makes intuitive sense as it is the solid-solid interaction between particles that are known to cause shear thickening in these JAM systems.

The nonlinearities within an oscillatory cycle can be further examined through thickening ratios shown in Fig. 17. The thickening ratio at medium strains was found to show shear-rate-thinning. At large strain-amplitudes, the thickening ratio remained shear-thinning even as both the dynamic viscosities transitioned to strain-rate thickening. This inconsistency is again a result of the details of the oscillatory cycle. Both η'_M and η'_L increase with applied strain, but the minimum strain-rate (maximum strain) viscosity η'_M

increases much more quickly resulting in a thinning within the cycle as the strain rate is increased, even though both viscosities show dramatic thickening when compared to the viscosity at small strains. A complete analysis of the viscous LAOS measurements for JAM indicates the observed nonlinearities are the result of a strong strain-thickening behavior across all the strains applied.

To summarize the LAOS behavior of JAM, the elastic nonlinearity with increasing strain amplitude was found to be strain/strain-rate softening behavior at applied strains just larger than the LVE limit, followed by a strong strain/strain-rate stiffening behavior at larger applied strains. The viscous nonlinearity initially showed strain/strain-rate thinning at small applied strains and evolved to strong strain/strain-rate thickening with increasing applied strain amplitude. The viscous non-linearities were dominated by strain thickening of the minimum strain-rate dynamic viscosity.

Conclusions

Large amplitude oscillatory shear behavior was investigated for three shear-thickening dispersions, $FLOC$, $HydroC$ and JAM, which shear-thicken by different mechanisms. The first material $FLOC$ shear-thickens due to shear-induced formation of particle clusters flocculated by polymer bridging. The second system $HydroC$, shear-thickens by the formation of hydroclusters. The third system JAM shear-thickens by jamming mechanism. The viscoelastic nonlinearities were examined through Lissajous-Bowditch plots and through local nonlinear measures of an oscillatory cycle such as, G'_M, G'_L, η'_M, and η'_L. The viscoelastic nonlinearities of the three shear-thickening systems are summarized in Table 1. The first harmonic moduli and the local nonlinear viscoelastic measures of the three systems are compared in Figs. 18 and 19 respectively.

The first harmonic moduli response of the three shear-thickening systems indicated that, at moderate strain-amplitudes, both $HydroC$ and JAM have exhibited strain/strain-rate softening and strain/strain-rate thinning behavior, associated microstructure alignment to the flow fields. However, the thinning/softening behavior of $HydroC$ was considerably less pronounced than JAM. While at large strain amplitudes, both $HydroC$ and JAM have showed strong strain/strain-rate stiffening and strain/strain-rate thickening behaviors associated with hydroclusters formation and the inter-particle jamming mechanisms. However, the stiffening/thickening in JAM was found to much more dramatic than $HydroC$ and larger by more than an order magnitude. The viscous nonlinearities of $HydroC$ and JAM were found to present strain and strain-rate thickening in good agreement with the steady-shear behavior. While the $FLOC$, in contrast, was found to show strain/strain-rate softening elastic nonlinearity throughout the nonlinear regime tested here. The viscous nonlinearity did exhibit a mild strain/strain-rate thickening at medium strain rates which could be due to dissipation of the equilibrium gel-like microstructure, but at large strain amplitudes, the behavior evolved to strain/strain-rate thinning associated with microstructure yielding. This response is quite different from the steady-shear behavior of $FLOC$. When the viscous nonlinearity of $FLOC$ is compared with steady shear, no strain-rate thickening was observed, even though the critical strain rates necessary for strain-thickening are achieved. The stress growth experiments indicated that large strains are required for strain-thickening to occur by the associated shear-induced polymer bridging mechanism, leading to this discrepancy.

Table 1 A tabulated summary of viscoelastic non-linearities of the three shear-thickening systems

Material	Mechanism	Frequency (rad/s)	Elastic nonlinearity		Viscous nonlinearity	
			G'_M and G'_L		η'_M and η'_L	
			Moderate strain	Large strain	Moderate strain	Large strain
$FLOC$	Shear-induced bridging	10 – 30	Strain softening and *strain-rate softening*	Strain softening and *strain-rate softening*	Strain thickening and *strain-rate thickening*	strain thinning and *strain-rate thinning*
$HydroC$	Hydrocluster	3	Strain softening and *strain-rate softening*	Strain stiffening and *strain-rate stiffening*	Strain thinning and strain-rate thinning	Strain thickening and *strain-rate thickening*
		10 – 30	Strain softening and Strain-rate softening	Strain stiffening and *strain-rate stiffening*	Strain thinning and strain-rate thinning	*Strain thickening* and strain-rate thickening
JAM	Jamming	10	Strain softening and *strain-rate softening*	Strain stiffening and *strain-rate stiffening*	Strain thinning and *strain-rate thinning*	*Strain thickening* and strain-rate thickening

The text highlighted in italic is the dominant non-linearity

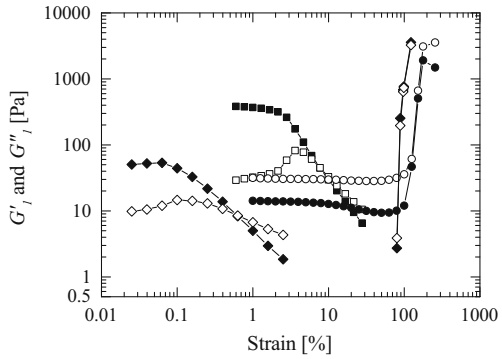

Fig. 18 A comparison of first harmonic moduli for the three dispersions (*black square*) $FLOC$, (*black circle*) $HydroC$ and (*black lozenge*) JAM. The data include storage modulus (*filled symbols*) and loss modulus (*hollow symbols*) as a function of strain amplitude at 10 rad/s

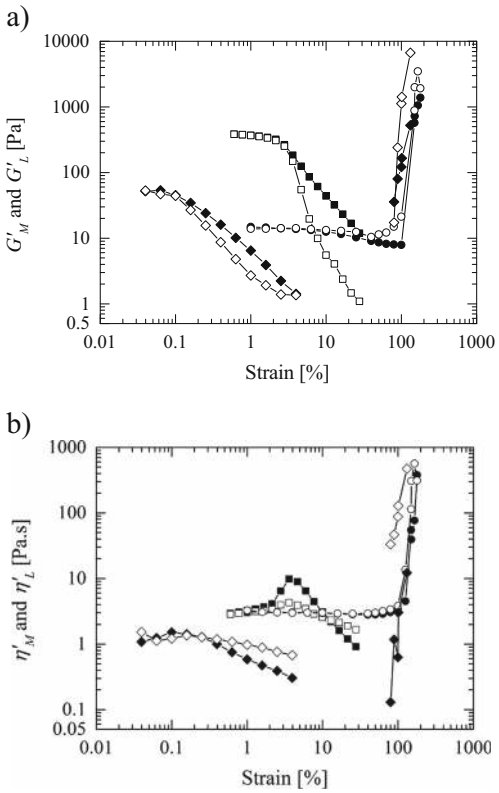

Fig. 19 A comparison of nonlinear viscoelastic measures as a function of strain amplitude at 10 rad/s for the three dispersions (*black square*) $FLOC$, (*black circle*) $HydroC$, and (*black lozenge*) JAM. The data include elastic measures, **a** G'_L (*filled symbols*) and G'_M (*hollow symbols*), and dynamic viscosity measures, **b** η'_L (*filled symbols*) and η'_M (*hollow symbols*)

However, both $HydroC$ and JAM were found to need relatively smaller strain amplitudes to induce shear-thickening by the associated mechanisms.

The nonlinear viscoelastic moduli, G'_M, G'_L, η'_M and η'_L were examined to study the effect of strain and strain-rate on viscoelastic nonlinearites within a given LAOS cycle. For all three shear-thickening systems, the trends of the nonlinear viscoelastic moduli with increasing strain amplitude were found to be qualitatively similar to the first harmonic moduli throughout the nonlinear range. However, the relative dominance of strain or strain-rates driving the viscoelastic nonlinearities has been found to vary between the shear-thickening systems, yielding a LAOS fingerprint that can be used to differentiate between the three different shear thickening mechanisms. A summary of these finding can be found in Table 1 with the dominant modes highlighted in italics. For all three shear-thickening systems, as seen in Fig. 19a, the elastic nonlinearities were found to be primarily driven by strain-rates rather than the strain amplitude. For the case of $FLOC$, the behavior was predominantly strain-rate softening throughout the nonlinear range. While for $HydroC$, the nonlinearity was very weak at moderate strain amplitudes. However, at large strain amplitudes, the strain-rate stiffening was found to be slightly more important than the strain-stiffening. For the case of JAM, the behaviors were predominantly strain-rate softening, followed by a strain-rate stiffening with increasing strain amplitude.

Similarly, the corresponding viscous nonlinearities were examined through dynamic viscosities, η'_M and η'_L, to study the relative importance of strain or strain-rates in the viscous nonlinearity of the three shear-thickening systems. A comparison of the viscous nonlinearities of all three systems is presented in Fig. 19b. The $FLOC$ was found to exhibit a predominantly strain-rate dominant viscous nonlinearity throughout the nonlinear regime. At medium strain amplitudes, the response was mildly strain-rate thickening. At large strain amplitudes, the behavior evolved to strain-rate thinning. For the case of $FLOC$, the viscous nonlinearities were found to be dominated by the effect of increasing strain-rates. While for $HydroC$ and JAM, the relative dominance of strain or strain-rate induced viscous non-linearity was found to depend on the strain amplitude and frequency. For the case of $HydroC$, at low frequency of $\omega = 3$ rad/s, the strain-rate thickening at large strain amplitudes was found to be a little larger than strain-thickening. While at higher frequency, $\omega > 3$ rad/s, the strain-thickening behavior was found to be modestly stronger than the strain-rate thickening. In both cases, the degree of strain and strain-rate thickening was essentially the same. For the case of JAM, at medium strain amplitudes, the behavior was predominantly strain-rate thinning. While at large strain amplitudes, the dominant behavior of JAM was strain thickening rather than strain-rate thickening. The predominant strain-induced thickening behavior at large strain amplitudes of JAM is similar to that of $HydroC$ observed at high frequencies. However, the magnitude of viscoelastic nonlinearities occurring within a LAOS cycle for the case

$HydroC$ were very much smaller than what was observed in the case of either $FLOC$ or JAM. In this LAOS study, we have observed strong differences in the viscoelastic nonlinearities of the three shear-thickening systems in both strain and strain-rate space, although they share a common shear-thickening feature in steady-shear. We believe this LAOS study offered valuable insights into the viscoelastic nonlinearities of three shear-thickening dispersions each with a different shear thickening.

Acknowledgments The authors would like to thank National Science of Foundation for funding the current project through the Center For Hierarchical Manufacturing at UMASS under grant number CMMI-1025020. We thank the reviewers for helpful suggestions in improving the discussions of the manuscript.

References

Atalik K, Keunings R (2004) On the occurrence of even harmonics in the shear stress response of viscoelastic fluids in large amplitude oscillatory shear. J Non-Newtonian Fluid Mech 122:107–116

Barnes H (1989) Shear-thickening (dilatancy) in suspensions of nonaggregating solid particles dispersed in newtonian liquids. J Rheol 33:329–366

Bertrand E, Bibette J, Schmitt V (2002) From shear thickening to shear-induced jamming. Phys Rev E 66:060,401

Bird RB, Armstrong RC, Hassager O (1987) Dynamics of polymeric liquids. Wiley, New York

Bischoff White EE, Chellamuthu M, Rothstein JP (2010) Extensional rheology of a shear-thickening cornstarch and water suspension. Rheol Acta 49:119–129

Bossis G, Brady JF (1984) Dynamic simulation of sheared suspensions. 1. General-method. J Chem Phys 80(10):5141–5154

Bossis G, Brady JF (1989) The rheology of Brownian suspensions. J Chem Phys 91(3):1866–1874

Bricker JM, Butler JE (2007) Correlation between stresses and microstructure in concentrated suspensions of non-brownian spheres subject to unsteady shear flows. Journal of Rheology (1978-present) 51(4):735–759

Brown E, Jaeger HM (2009) Dynamic jamming point for shear thickening suspensions. Phys Rev Lett 103:086,001

Cates M, Haw M, Holmes C (2005) Dilatancy, jamming, and the physics of granulation. J Phys Condens Matter 17:S2517–S2531

Chang L, Friedrich K, Schlarb A, Tanner R, Ye L (2011) Shear-thickening behaviour of concentrated polymer dispersions under steady and oscillatory shear. J Mater Sci 46(2):339–346

Chellamuthu M, Arndt E, Rothstein JP (2009) Extensional rheology of shear-thickening nanoparticle suspensions. Soft Matter 5:2117–2124

Cho KS, Hyun K, Ahn KH, Lee SJ (2005) A geometrical interpretation of large amplitude oscillatory shear response. J Rheol 49(3):747–758

Ewoldt R, Bharadwaj N (2013) Low-dimensional intrinsic material functions for nonlinear viscoelasticity. Rheol Acta 52(3):201–219

Ewoldt RH, Hosoi AE, McKinley GH (2008) New measures for characterizing nonlinear viscoelasticity in large amplitude oscillatory shear. J Rheol 52(6):1427–1458

Fall A, Huang N, Bertrand F, Ovarlez G, Bonn D (2008) Shear thickening of cornstarch suspensions as a reentrant jamming transition. Phys Rev Lett 100:018,301

Fall A, Lemaître A, Bertrand F, Bonn D, Ovarlez G (2010) Shear thickening and migration in granular suspensions. Phys Rev Lett 105:268

Fischer C, Plummer C, Michaud V, Bourban PE, Mnson JA (2007) Pre- and post-transition behavior of shear-thickening fluids in oscillating shear. Rheol Acta 46(8):1099–1108

Foss DR, Brady JF (2000) Structure, diffusion and rheology of brownian suspensions by stokesian dynamics simulation. J Fluid Mech 407:167–200

Frith WJ, d'Haene P, Buscall R, Mewis J (1996) Shear thickening in model suspensions of sterically stabilized particles. J Rheol 40(4):531–548

GadalaMaria F, Acrivos A (1980) Shear-induced structure in a concentrated suspension of solid spheres. J Rheol (1978-present) 24(6):799–814

Galindo-Rosales F, Rubio-Hernàndez FJ (2010) Static and dynamic yield stresses of Aerosil®200 suspension in polypropylene glycol. App Rheol 20:22, 787

Graham MD (1995) Wall slip and the nonlinear oscillatory dynamics of large amplitude shear flows. J Rheol 39(4):697–712

Helber R, Doncker F, Bung R (1990) Vibration attenuation by passive stiffness switching mounts. J Sound Vibration 138(1):47–57

Hoffman RL (1972) Discontinuous and dilatant viscosity behavior in concentrated suspensions. i. observation of a flow instability. J Rheol 16:155–173

Hyun K, Nam GJ, Wilhellm M, Ahn KH, Lee SJ (2006) Large amplitude oscillatory shear behavior of PEO-PPO-PEO triblock copolymer solutions. Rheol Acta 45:239–249

Hyun K, Wilhelm M, Klein CO, Cho KS, Nam JG, Ahn KH, Lee SJ, Ewoldt RH, McKinley GH (2011) A review of nonlinear oscillatory shear tests: Analysis and application of large amplitude oscillatory shear (laos). Prog Polym Sci 36(12):1697–1753

Hyun K, Nam GJ, Wilhelm M, Ahn KH, Lee SJ (2003) Nonlinear response of complex fluids under laos (large amplitude oscillatory shear) flow. Korea-Australia Rheology Journal 15(2):97–105

Jiang W, Sun Y, Xu Y, Peng C, Gong X, Zhang Z (2010) Shear-thickening behavior of polymethylmethacrylate particles suspensions in glycerine water mixtures. Rheol Acta 49(11–12):1157–1163

Kamibayashi M, Ogura H, Otsubo Y (2008) Shear-thickening flow of nanoparticle suspensions flocculated by polymer bridging. J Colloid Interface Sci 321(2):294–301

Kawaguchi M, Yamamoto T, Kato T (1996) Rheological studies of hydrophilic and hydrophobic silica suspensions in the presence of adsorbed poly(N-isopropylacrylamide). Langmuir 12: 6184–6187

Khandavalli S, Rothstein JP (2014) Extensional rheology of shear-thickening fumed silica nanoparticles dispersed in an aqueous polyethylene oxide solution. J Rheol 58(2):411–431

Klein C, Venema P, Sagis L, Linden vd E (2008) Rheological discrimination and characterization of carrageenans and starches by Fourier transform-rheology in the non-linear viscous regime. J Non-Newtonian Fluid Mech 151:145–150

Larsen R, Kim JW, Zukoski C, Weitz D (2014) Fluctuations in flow produced by competition between apparent wall slip and dilatancy. Rheologica Acta 53(4):333–347

Larsen RJ, Kim JW, Zukoski CF, Weitz DA (2010) Elasticity of dilatant particle suspensions during flow. Phys Rev E 81:011,502

Larson RG (1999) The structure and rheology of complex fluids. Oxford University Press, Newyork

Laun HM, Bung R, Schmidt F (1991) Rheology of extremely shear thickening polymer dispersions (passively viscosity switching fluids). J Rheol 35(6):999–1034

Laun HM, Bung R, Hess S, Loose W, Hess O, Hahn K, Hadicke E, Hingmann R, Schmidt F, Lindner P (1992) Rheological and

small-angle neutron-scattering investigation of shear-induced particle structures of concentrated polymer dispersions submitted to plane poiseuille and couette-flow. J Rheol 36(4):743–787

Leblanc JL (2008) Large amplitude oscillatory shear experiments to investigate the nonlinear viscoelastic properties of highly loaded carbon black rubber compounds without curatives. J App Polym Sci 109(2):1271–1293

Leblanc JL, Putman M, Pianhanuruk E (2011) A thorough study on the relationships between dispersion quality and viscoelastic properties in carbon black filled SBR compounds. J App Polym Sci 121:1096–1117

Lee M, Alcoutlabi M, Magda JJ, Dibble C, Solomon MJ, Shi X, McKenna GB (2006) The effect of the shear-thickening transition of model colloidal spheres on the sign of n1 and on the radial pressure profile in torsional shear flows. J Rheol 50(3):293–311

Lee Y, Wagner N (2003) Dynamic properties of shear thickening colloidal suspensions. Rheologica Acta 42(3):199–208

Lin Y, Phan-Thien N, Khoo BC (2013) Short-term and long-term irreversibility in particle suspensions undergoing small and large amplitude oscillatory stress. J Rheol 57(5):1325–1346

Lootens D, van Damme H, Hémar Y, Hébraud P (2005) Dilatant flow of concentrated suspensions of rough particles. Phys Rev Lett 95:268,302

Mason TG, Weitz DA (1995) Linear viscoelasticity of colloidal hard sphere suspensions near the glass transition. Phys Rev Lett 75:2770–2773

Melrose JR, Ball RC (2004) Continuous shear thickening transitions in model concentrated colloids—the role of interparticle forces. J Rheol 48(5):937–960

Merger D, Wilhelm M (2014) Intrinsic nonlinearity from laos train experiments on various strain- and stress-controlled rheometers: a quantitative comparison. Rheol Acta 53:621–634

Mewis J, Biebaut G (2001) Shear thickening in steady and superposition flows effect of particle interaction forces. J Rheol 45(3):799–813

Mewis J, Vermant J (2000) Rheology of sterically stabilized dispersions and latices. Prog Org Coat 40:111–117

Nam J, Ahn K, Lee S, Hyun K (2011) Strain stiffening of non-colloidal hard sphere suspensions dispersed in newtonian fluid near liquid-and-crystal coexistence region. Rheol Acta 50 (11–12)

Narumi T, See H, Suzuki A, Hasegawa T (2005) Response of concentrated suspensions under large amplitude oscillatory shear flow. J Rheol 49(1):71–85

Neidhfer T, Sioula S, Hadjichristidis N, Wilhelm M (2004) Distinguishing linear from star-branched polystyrene solutions with fourier-transform rheology. Macromol Rapid Commun 25: 1921–1926

Nilsson MA, Kulkarni R, Gerberich L, Hammond R, Singh R, Rothstein JP (2013) The effect of fluid rheology on enhanced oil recovery using a microfluidic sandstone device. Submitted to J Non-Newtonian Fluid Mech

O'Brien VT, Mackay ME (2000) Stress components and shear thickening of concentrated hard sphere suspensions. Langmuir 16(21):7931–7938

Otsubo Y (1993) Size effects on the shear-thickening behavior of suspensions flocculated by polymer bridging. J Rheol 37: 799–809

Otsubo Y (1999) A nonlinear elastic model for shear thickening of suspensions flocculated by reversible bridging. Langmuir 15(6):1960–1965

Otsubo Y (2001) Rheology of colloidal suspensions flocculated by reversible bridging. Chem Eng Sci 56(9):2939–2946

Otsubo Y, Umeya K (1984) Rheological properties of silica suspensions in polyacrylamide solutions. J Rheol 28(2):95–108

Raghavan S, Khan S (1997) Shear-thickening response of fumed silica suspensions under steady and oscillatory shear. J Colloid and Interface Sci 185:57–67

Raghavan SR, Khan SA (1995) Shear-induced microstructural changes in flocculated suspensions of fumed silica. J Rheol 39(6): 1311–1325

Raghavan SR, Walls HJ, Khan SA (2000) Rheology of silica dispersions in organic liquids: new evidence for solvation forces dictated by hydrogen bonding. Langmuir 16(21):7920–7930

Seto R, Mari R, Morris JF, Denn MM (2013) Discontinuous shear thickening of frictional hard-sphere suspensions. Phys Rev Lett 111:218,301

Shenoy S, Wagner N (2005) Influence of medium viscosity and adsorbed polymer on the reversible shear thickening transition in concentrated colloidal dispersions. Rheol Acta 44: 360–371

Sun W, Yang Y, Wang T, Liu X, Wang C, Tong Z (2011) Large amplitude oscillatory shear rheology for nonlinear viscoelasticity in hectorite suspensions containing poly(ethylene glycol). Polymer 52:1402–1409

Voronin E, Gun'ko V, Guzenko N, Pakhlov E, Nosach L, Leboda R, Skubiszewska-Ziba J, Malysheva M, Borysenko M, Chuiko A (2004) Interaction of poly(ethylene oxide) with fumed silica. J Colloid and Interface Sci 279(2):326–340

Wagner NJ, Brady JF (2009) Shear thickening in colloidal dispersions. Physics Today 62(10):27–32

Wilhelm M, Marin D, Spiess HW (1998) Fourier-transform rheology. Rheol Acta 37:399–405

Wilhelm M, Reinheimer P, Ortseifer M (1999) High sensitivity fourier-transform rheology. Rheol Acta 38:349–356